Materials Science in Semiconductor Processing 107 (2020) 104836

Contents lists available at ScienceDirect

Materials Science in Semiconductor Processing

journal homepage: http://www.elsevier.com/locate/mssp

Inducing a level inside of CdTe bandgap doping with Sn using a co-sublimation technique by CSS

J.A. Ríos-González [a,*], R. Mis-Fernández [a], E. Camacho-Espinosa [a], I. Riech [b], E. Menéndez-Proupin [c], M.A. Flores [d], W. Orellana [e], J.L. Peña [a]

[a] Departamento de Física Aplicada. Centro de Investigación y de Estudios Avanzados del IPN Unidad Mérida. Carretera Antigua a Progreso Km 6, A. P. 73, Cordemex, 97310, Mérida, Yucatán, Mexico
[b] Laboratorio de Ciencias de Materiales, Facultad de Ingeniería, Universidad de Yucatán, CP 97130, Mérida, Yucatán, Mexico
[c] Departamento de Física, Facultad de Ciencias, Universidad de Chile, Las Palmeras 3425, 780-0003, Ñuñoa, Santiago, Chile
[d] Facultad de Ingeniería y Tecnología, Universidad San Sebastián, Bellavista 7, Santiago, 8420524, Chile
[e] Departamento de Ciencias Físicas, Universidad Andres Bello, Sazié 2212, Santiago, 0370136, Chile

ARTICLE INFO

Keywords:
Intermediate band
Doping
Low-cost
Closed-spaced sublimation

ABSTRACT

In this work, cadmium telluride (CdTe) thin films were doped with Sn using a low-cost co-sublimation technique by a homemade close-spaced sublimation (CSS) system. Sn amount was calculated to obtain CdTe film doped with a percentage content lower than 0.4 at%. Chemical, structural, morphological, and optical properties of the as-deposited CdTe (u-CdTe) and Sn-doped CdTe (t-CdTe) films were measured and compared. Raman and XPS characterization showed the presence of Sn in t-CdTe thin films and XRD analysis revealed a strong signal related to CdTe planes (220) and (311) and in a lesser extent a signal related to SnTe. Irregular shaped grains with similar size related to Sn incorporation in the films were found with FE-SEM technique. Photoluminescence spectrum indicates an energy band at 0.7 eV, generating a band inside of CdTe bandgap, due to defects induced by the Sn in CdTe lattice, matching with a theoretical study. The changes observed in Sn doped CdTe film suggest that it can be used for optoelectronics applications.

1. Introduction

CdTe is a material with a high absorption coefficient, which can be used for different technological applications such as solar cells and detectors. Depending on the application it is desirable to dope the CdTe, in order to change its properties. However, it has been a hard work due to its native defects, for instance, the Cd vacancy (V_{Cd}), Te antisite (Te_{Cd}), and Te interstitial (Te_i) [1,2]. CdTe doping has been performed using different elements such as Sb [3], P [4], O [5], Bi [6], Cu [7], As [8], etc. Among these materials, Sn can occupy the Cd position in CdTe lattice inducing an isolate intermediate band (IB) close to the midgap [9,10]. This consideration makes Sn a promising doping material for intermediate band solar cells applications because it could allow a photoexcitation process in two steps i.e. from valence band (VB) to the conduction band (CB) and VB → IB → CB [11].

Inducing an IB into a semiconductor allows electron transitions in and out of the IB. However, it could act as recombination centers (deep energy traps) [12,13], for this reason, the IB potential depends on the photogeneration-recombination probability [14]. Luque et al. [15], compared the non-radiative recombination rates of intermediate band versus isolated deep levels. They mention that it is possible to suppress the recombination mechanism by increasing the density of impurities to avoid strong localized charge variations, inducing only a level of sub-bandgap optical absorption. However, for CdTe, non-radiative recombination always is present and only it can be reduced. To achieve an IB, it is necessary careful doping control. In fact, there is a minimum and maximum doping level required to create the IB. Low doping concentrations generate radiative and non-radiative recombination centers, which can contribute to losses in photogenerated current. On the other hand, high doping concentrations can be distributed in CdTe grain boundaries or forming agglomerations, compensating the doping effect induce carriers degradation [6,16].

The CdTe doping has been done mainly using high precision and expensive techniques such as the Bridgman method and molecular beam epitaxy [6,17–19]. In Bridgman technique, Cd and Te are placed in quartz ampoule, adding the dopant directly to the CdTe powder or with

* Corresponding author.
E-mail address: juan.rios@cinvestav.mx (J.A. Ríos-González).

https://doi.org/10.1016/j.mssp.2019.104836
Received 19 August 2019; Received in revised form 25 October 2019; Accepted 8 November 2019
Available online 16 November 2019

a previous mixing process, thus, the dopant atoms are randomly positioned. For this reason, it is necessary to add small quantities of Sn in the CdTe, in this way, the Sn should be positioned with V_{Cd} defect creating the substitutional Sn impurity (Sn_{Cd}). In this work, we design a low-cost close-spaced sublimation (CSS) system with the purpose of dope CdTe with Sn and induce an intermediate band. The thin films of Sn-doped CdTe were characterized focusing on the chemical, structural, morphological, and optical properties.

2. Experimental

2.1. Thin film deposition

A homemade CSS system was developed to incorporate Sn in CdTe film. The deposition system consists of three graphite parts which are Sn dopant crucible, CdTe source container, and substrate holder. The CdTe source container has a perforation in the middle to let pass the Sn from the dopant crucible to the substrate holder. In order to avoid heat transfer from the CdTe source container to the Sn dopant crucible, ceramic spacers were placed between them. The heat source for the CSS system is composed of halogen lamps as indicated in Fig. 1. The temperature of the CdTe source, the Sn dopant crucible, and the substrate holder was measured with K-type thermocouples placed inside each graphite achieving in this way accurate temperature measurements.

In order to determine the amount of Sn necessary to dope CdTe, this work was based on the theoretical study of Flores et al. [9], were 0.4 at% of Sn was considered to induce an IB. Here, $SnCl_2$ pellets were used as a source of Sn. The amount of $SnCl_2$ was optimized to obtain a range of 0.2–0.4 at% of Sn in the thin film. Hence, the pellet preparation consisted of milling 0.13 g of $SnCl_2$ in an agate mortar until a fine powder was obtained. After, the powder was inserted in a pellet die and pressed with 5 Ton, until a solid piece was obtained. The pellet of $SnCl_2$ was placed in the center of the dopant crucible as is showed in Fig. 1.

The low sublimation temperature of $SnCl_2$ allows its incorporation in the CdTe film by CSS. The vapor pressure data for $SnCl_2$ can be obtained from thermodynamics tables [20], however, the work pressure of sublimation deposition of CdTe (0.5 mbar) is not present in the tables. Nevertheless, the sublimation temperature can be estimated from the Clausius-Clapeyron equation:

$$ln(P/P_0) = -\left(\Delta H_{vap}\right)/R\,(1/T - 1/T_0),$$

setting P_0 and T_0 as known values from the thermodynamic table, P is the work pressure and its corresponding temperature T, ΔH_{vap} and R are the enthalpy of vaporization and gas constant, respectively. As a result, the sublimation temperature of $SnCl_2$ is ~290 °C.

Both undoped CdTe (u-CdTe) and tin-doped CdTe (t-CdTe) were deposited on soda-lime glass previously cleaned with neutral detergent solution in an ultrasonic bath, rinsed with de-ionized water and dried with air. The vacuum chamber was air evacuated to a base pressure of 1.3×10^{-5} mbar. Then, Ar was introduced into the chamber setting pressure of 0.5 mbar in dynamic vacuum. The CdTe source temperature was gradually increased to 550 °C, according to ramp showed in Fig. 2, once this value was reached, the CdTe sublimation started. After 6 min, $SnCl_2$ sublimation begins to incorporate Sn into the middle of the CdTe film. Doping was previously optimized to promote Sn diffusion through the film. The total sublimation time was 12 min, then, the process was quickly stopped by introducing Ar at 5.3 mbar pressure.

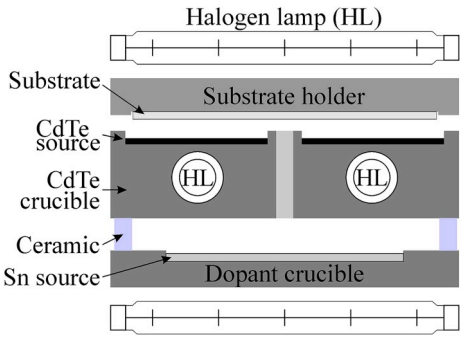

Fig. 1. Schematic view of the close-spaced sublimation system.

2.2. Characterization techniques

Raman spectra were carried out with a WITec Raman confocal coupled with AFM with the excitation wavelength of 488 nm, measuring a line scan in z-axes direction from (x, y, 0) to (x, y, -3.5) (in μm). The crystalline structure was identified by X-ray diffraction (Siemens D5000 diffractometer) using a Cu Kα radiation (λ = 1.5405 Å) beam. The measurements were recorded in a 2θ diffraction angle ranging from 20° to 80° in steps of 0.02°. Composition of t-CdTe was measured by XPS analysis in a K-Alpha equipment by Thermo Fischer Scientific with an Al X-ray source; spectra were calibrated by using the C1s emission at 284.6 eV. The surface and cross-sectional morphology were analyzed by a Jeol 7600F FE-SEM in LEI mode, with an energy of 5 kV. The photoluminescence spectra were carried out using an Acton monochromator with InGaAs infrared detector. The samples were analyzed at low temperature (21 K) and the 488 nm line of Ar laser was used as excitation source.

3. Results and discussion

3.1. Structural properties

In order to observe Sn sublimation, a $SnCl_2$ pellet was sublimated on a glass substrate. XRD confirmed the alpha-tin phase in the substrate (not shown here for brevity). The $SnCl_2$ dissociates into its elements, $SnCl_2(s) \rightarrow Sn(g) + Cl_2\uparrow(g)$. Once the Cl_2 is formed, it is evacuated due to dynamic vacuum in the sublimation process, leaving the tin, which is incorporated in the CdTe lattice.

Raman depth profile was carried out to determine t-CdTe film composition. Fig. 3a shows the Raman depth profile through the t- CdTe film, showing that CdTe peak is weak and wider at the film surface (red line) due to surface contamination and unfocused Raman laser. The CdTe and Te peaks become more intense as the "Z scan" move depth into the sample. At ~2.5 μm depth, the mean peak (121 cm^{-1}) belonging to A_1(Te) symmetry, shifts downwards. Using the equation of the classical vibration model [21], $\bar{\nu} \propto (k_0/\mu)^{1/2}$, where $\bar{\nu}$ is the vibrational frequency, k_0 is the bond force constant and μ is the reduced mass, it can be deduced that if Sn substitutes Cd, the reduced mass increases because Sn is a heavier atom (i.e. $\mu_{Cd} < \mu_{Sn}$), therefore $\bar{\nu}$ value decrease, resulting in Raman peak shift to lower frequency, which is clearly observed.

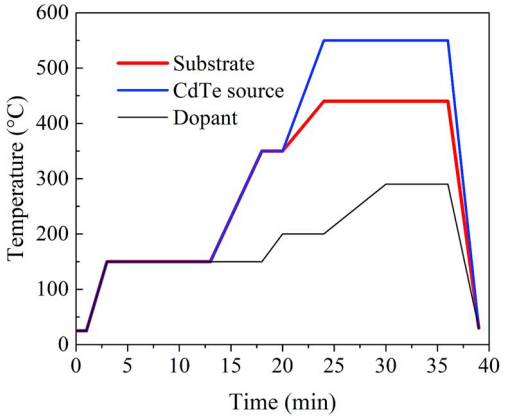

Fig. 2. Temperature ramp of t-CdTe deposition.

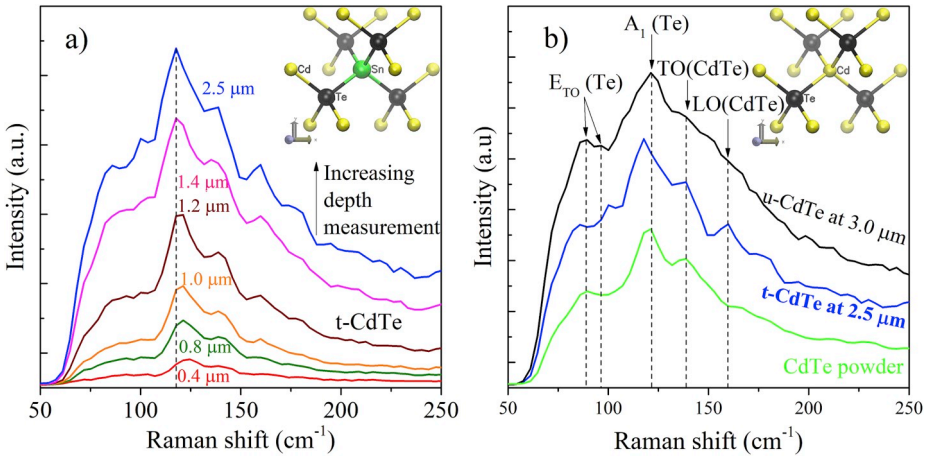

Fig. 3. a) Raman depth profile of t-CdTe (inset is CdTe representation with Sn in the position of Cd), b) comparison between u-CdTe, t-CdTe and CdTe powder (inset shows the CdTe bonds).

Fig. 3b shows the Raman spectra of the CdTe powder (Sigma-Aldrich 99.99%), u-CdTe, and t-CdTe. The dashed lines indicate the characteristic peak positions of the CdTe and Te in Raman spectra. In t-CdTe sample appear peaks corresponding to the Transverse Optical (TO) phonon of elemental Te identified at Raman shift wavenumber 89 and 96 cm^{-1} [22]. Also, u-CdTe presents both elemental Te peaks, it is due to the formation of microcrystals of Te into CdTe during the deposition process according to Ref. [23]. On the other hand, CdTe powder shows only the peak at 89 cm^{-1}. As it was previously described, the peak corresponding to A_1(Te) shifted to the left in the t-CdTe sample. The characteristic peaks at 138 and 160 cm^{-1} correspond to the TO(CdTe) and the LO(CdTe) [24,25], respectively. The molecular representations in the insets in Fig. 3 show the possible arrangement of u-CdTe and t-CdTe. As can be seen, the interchange between atoms generates changes in the vibration modes detected by Raman spectroscopy [26].

In this work, Bragg-Brentano configuration was used to perform XRD measurements with the purpose of obtaining CdTe bulk information, which is more useful in this case [27]. Fig. 4 shows the XRD patterns of t-CdTe and u-CdTe with the main peaks corresponding to (220), (311) and (111) planes according to JCPDS card 15–0770 for both samples. The inset shows a zoom in the region corresponding to SnTe peaks (20°–50°). In the zoom of the XRD patterns, it can be observed small peaks corresponding to (220) and (200) planes of the SnTe according to the JCPDS card 46–1210 for t-CdTe sample.

Fig. 5 shows survey XPS spectra scan of t-CdTe and the inset shows low-intensity peak deconvolution of Sn ($3d_{3/2}$ and $3d_{5/2}$). The relative wide FWHM shows the presence of both peaks with Sn^{2+} and Sn^{4+} states. The concentration of Sn on CdTe film surface was 0.4 at.% measured with XPS. After 30, 60, 500 and 1500 s of erosion, the Sn concentration drops to 0.2 at%. As can be seen in Table 1, the sample has more tin content at the surface probably due to the resublimation, however, the concentration of Sn remains through the sample. Also, it was found oxygen and carbon probably due to the presence of CO_2, after being exposed to the environment. The $SnCl_2$ co-sublimation allows the introduction of Sn into the CdTe lattice inducing the formation of different defects, such the Sn interstitial (Sn_i), Sn in the position of Cd (Sn_{Cd}), and Sn in the position of Te (Sn_{Te}). In addition, XPS measurements indicate that the atomic percentage of Cd is greater than Te, both in u-CdS as t-CdTe, making a CdTe with Cd-rich conditions. In both

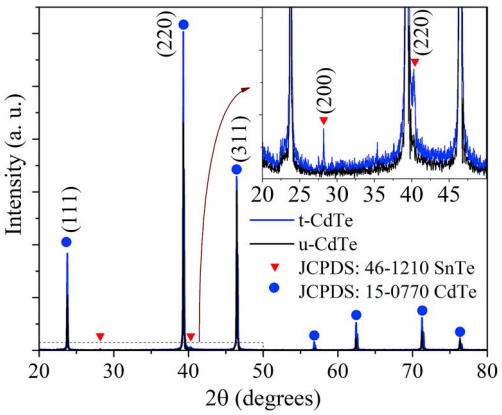

Fig. 4. XRD patterns of t-CdTe. The inset shows the zoom to see the SnTe peaks.

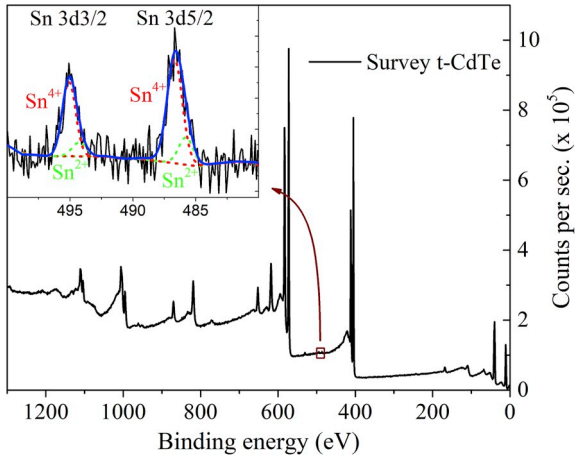

Fig. 5. XPS spectra of survey of t-CdTe. The inset shows the deconvolution of $Sn3d_{3/2}$ and $Sn3d_{5/2}$ core level for high-resolution XPS.

Table 1
Atomic percentage of the t-CdTe film superficially, with 30, 60, 500, and 1500 s of erosion.

Element	Atomic %				
	Surface	30 s erosion	60 s erosion	500 s erosion	1500 s erosion
Cd 3d	19.02	44.97	46.58	47.70	49.08
Te 3d	16.49	42.42	45.23	46.73	47.95
Sn 3d	0.39	0.22	0.23	0.25	0.26
C 1s	41.42	5.28	3.41	2.40	1.65
O 1s	21.37	6.63	4.48	2.87	1.00
Cl 2p	1.31	0.48	0.07	0.05	0.06

samples are expected a high resistance since they are grown in oxygen absence [28] and the deviation from stoichiometry in Cd–Te ratio [29]. According to the calculations in Refs. [7,30], the formation energy for CdTe with Cd-rich conditions, the most probable defects are Sn_i and Sn_{Cd}. This implies that Sn is bonding with Te, in line with the XRD and Raman results.

3.2. Morphological results

Fig. 6 shows the top view FE-SEM micrographs of u-CdTe (a) and t-CdTe (b). The u-CdTe sample has irregular granular structures with big grains (inset), homogeneous surface, and without cracks or pinholes, while the t-CdTe sample presents smaller grains (inset), with homogeneous surface and small voids. The cross-section micrographs (Fig. 6c and d) demonstrate a morphological change between u-CdTe and t-CdTe during the crystal growth. A reduction of grain size is observed when CdTe is co-sublimated with Sn, which is probably due to nucleation of CdTe interacting with the Sn, as it was similarly observed in Ref. [31]. It should be noted that in u-CdTe, grains seem compact, that is without voids and stacking faults, but when Sn is added, it is formed an uncompensated material where voids appear in the film principally due to the stress caused during the grains growth and the non-homogeneity nucleation in the glass. The thickness of both samples was approximately 3.5 μm.

3.3. Optical properties

In order to examine the energy states inside of CdTe bandgap, photoluminescence (PL) analysis was performed, as shown in Fig. 7a. According to PL results, u-CdTe presented an asymmetric peak which can be deconvoluted in two bands at 0.714 and 0.733 eV, it could be due to the antisite defect Te_{Cd} [2,32]. For t-CdTe, an intense band was observed at 0.707 eV and a lower intensity peak at 0.789 eV. The theoretical calculation reported in Ref. [9] indicates that the IB in the Sn-doped CdTe is present in the middle of the bandgap and Sn 5s orbital is the main contribution. The band obtained in this work for t-CdTe film at 0.707 eV, suggests that the transition occurs from IB to VB and it can be explained by the electron transition as shown in the inset of Fig. 7 a.

XPS deconvolution indicates the presence of Sn^{2+} and Sn^{4+} which agrees with the k-resolved total density of states in Ref. [9]. When Sn is bonded with Te, it is generated a delocalization of 5s orbital which origin the IB since the 5s orbitals become in extended states and they are hybridized with Te 5p orbitals, for this reason, is obtained the Sn^{4+} with a higher proportion in XPS. Additionally, Fig. 7b shows the imaginary part of the dielectric function calculated using a $3 \times 3 \times 3$ CdTe supercell using a single Sn atom impurity in Cd position. The dielectric function was computed within the GW-RPA approximation, i.e., without exciton effects, using a $6 \times 6 \times 6$ k-point mesh displaced by (0.11,0.12,0.13) in reciprocal coordinates. Other parameters are the same as Ref. [9]. While this calculation is not completely converged with respect to the number of k-points, it allows clarifying the origin of the observed PL peaks.

In Fig. 7b, the black line represents the case of empty IB, where the transitions VB → IB cause the peak at 0.7 eV which is completely consistent whit the PL result. The red line represents the case with the IB fully-occupied, where VB → IB transitions are forbidden by the Pauli exclusion principle, but IB → CB transitions are possible. However, the IB → CB transitions do not show up in the computed spectrum, because they are forbidden by symmetry. This can be understood with the help of the k-resolved density of states (Fig. 3 of Ref. [9]), which shows that the IB and CB have nearly the same dispersion near the Γ point, and both are projected on cation 5s orbitals. The computed imaginary part of the dielectric function is proportional to the absorption coefficient $\sigma(\hbar\omega)$, which in turn is related to the PL intensity by Ref. [33]:

$$\Im(\hbar\omega) = \frac{n^2(\hbar\omega)^2}{\pi^2\hbar^3c^2}\sigma(\hbar\omega)f_u(1-f_l),$$

where f_l and f_u are the occupations of the lower and upper bands, respectively, participating in absorption and PL. This suggests that the predominant transition observed in PL is IB → VB. With these localized states in the middle of CdTe bandgap, it is possible to obtain three different photon absorption stages, VB → CB, VB → IB, and IB → CB, matching with the theoretical results.

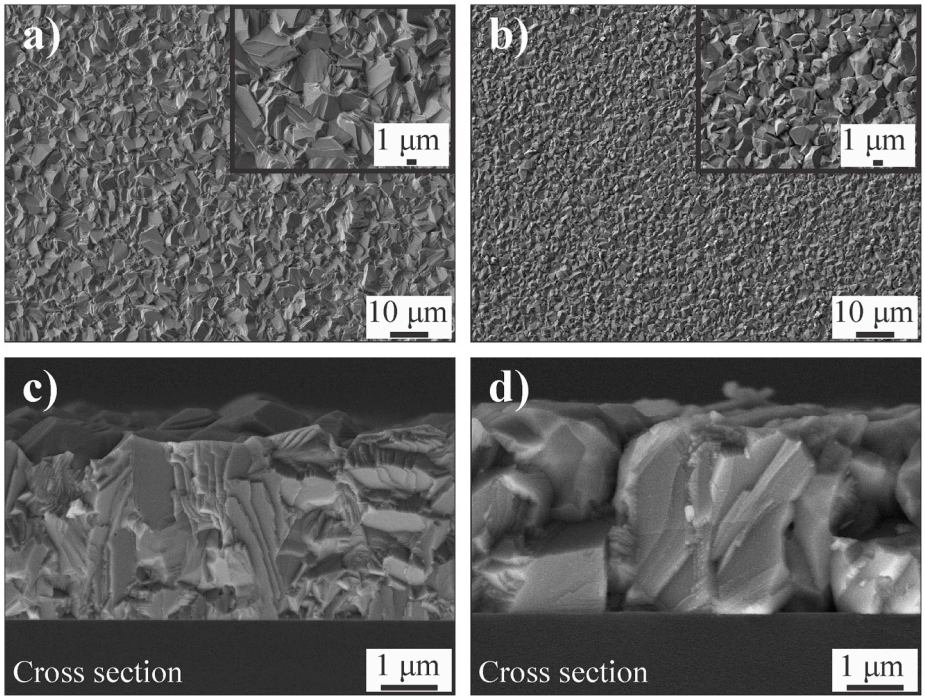

Fig. 6. FE-SEM micrographs: surface of a) u-CdTe and b) t-CdTe; c) and d) show the cross-section of u-CdTe and t-CdTe, respectively.

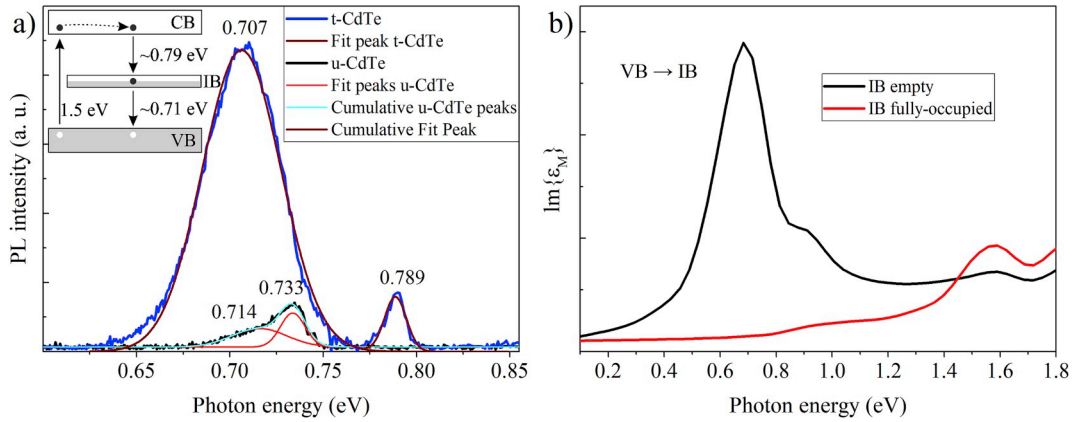

Fig. 7. a) PL spectra of t-CdTe and u-CdTe samples at 21 K. The inset shows schematic band structure. b) Imaginary part of dielectric function calculated for Sn_{Cd} defect in a 54-atom supercell of CdTe.

4. Conclusions

The presence of tin was confirmed by Raman, XPS, and XRD techniques, concluding that the doping of CdTe was successfully achieved, showing that it is possible to dope the CdTe with a low-cost technique as CSS. XRD pattern revealed the presence of SnTe in the t-CdTe sample with small peaks corresponding to (220) and (200) planes, without change the CdTe phase. Additionally, FE-SEM images revealed changes in grain size after Sn incorporation in the CdTe films. Voids were also found, presumably due to stress during the CdTe crystal growth. XPS technique shows the presence of Sn^{2+} and Sn^{4+}, being the tin atomic percentage equal to 0.4 at % at the surface, which drops to 0.2 at.% after erosion. The PL spectrum confirmed the theoretical prediction of a band in the middle of the CdTe bandgap, showing a strong emission line at 0.707 eV. This state could induce sub-bandgap optical absorption reducing the recombination mechanisms. Further investigations can be applied to this material for applications in detectors or solar cells.

Declaration of competing interest

The authors declare that they have no known competing financial interests or personal relationships that could have appeared to influence the work reported in this paper.

Acknowledgments

This work has been supported by CONACYT-SENER (México) under projects CeMiE-Sol 207450/P25 and Consolidación del Laboratorio de Energía Renovable del Sureste (LENERSE) 254667 (México). Measurements were performed at LANNBIO CINVESTAV-IPN Mérida under projects FOMIX-Yucatán 2008–108160, CONACYT LAB-2009-01-123913, 292692, 294643, 188345 y 204822 (México). The authors thank to W. Cauich, J. Bante, and D. Quintanilla for technical assistant. W. O. acknowledges support from CONICYT/FONDECYT (Chile), through Grant No. 1170480. E. M-P acknowledges support from grant CONICYT/FONDECYT (Chile) Regular 1171807. Powered@NLHPC: This research was partially supported by the supercomputing infrastructure of the NLHPC (ECM-02) (Chile). J. A. R-G acknowledges financial support from CONACyT (México) for the scholarship.

Appendix A. Supplementary data

Supplementary data to this article can be found online at https://doi.org/10.1016/j.mssp.2019.104836.

References

[1] J.L. Roehl, S.V. Khare, Diffusion of Cd vacancy and interstitials of Cd, Cu, Ag, Au and Mo in CdTe: a first principles investigation, Sol. Energy 101 (2014) 245–253, https://doi.org/10.1016/j.solener.2013.12.017.
[2] M. Fiederle, A. Fauler, J. Konrath, V. Babentsov, J. Franc, R.B. James, Comparison of undoped and doped high resistivity CdTe and (Cd,Zn)Te detector crystals, IEEE Trans. Nucl. Sci. 51 (2004) 1864–1868, https://doi.org/10.1109/NSSMIC.2003.1352661.
[3] A. Zhao, A. Farah, D. Morel, C.S. Ferekides, The effect of impurities on the doping and Voc of CdTe/CdS thin film solar cells, Thin Solid Films 517 (2009) 2365–2369, https://doi.org/10.1016/j.tsf.2008.11.041.
[4] J.M. Burst, J.N. Duenow, D.S. Albin, E. Colegrove, M.O. Reese, J.A. Aguilar, C.-S. Jiang, M.K. Patel, M.M. Al-Jassim, D. Kuciauskas, S. Swain, T. Alekim, K.G. Lynn, W.K. Metzger, CdTe solar cells with open-circuit voltage breaking the 1 V barrier, Nat. Energy 1 (2016) 16015, https://doi.org/10.1038/nenergy.2016.15.
[5] N.E. Gorji, Deposition and doping of CdS/CdTe thin film solar cells, J. Semicond. 36 (2015), https://doi.org/10.1088/1674-4926/36/5/054001, 054001.
[6] O. Vigil-Galán, M. Courel, F. Cruz-Gandarilla, D. Seuret-Jiménez, CdTe:Bi films deposited by closed space vapor transport under variable pressure and doping levels: evidences of the possible formation of an intermediate band, J. Mater. Sci. Mater. Electron. 27 (2016) 6088–6095, https://doi.org/10.1007/s10854-016-4534-1.
[7] T.D. Dzhafarova, S.S. Yesilkayaa, N. Yilmaz Canlia, M. Caliskan, Diffusion and influence of Cu on properties of CdTe thin films and CdTe/CdS cells, Sol. Energy Mater. Sol. Cells 85 (2005) 371–383, https://doi.org/10.1016/j.solmat.2004.05.007.
[8] A. Nagaoka, D. Kuciauskas, M.A. Scarpulla, Doping properties of cadmium-rich arsenic-doped CdTe single crystals: evidence of metastable AX behavior, Appl. Phys. Lett. 111 (2017) 232103, https://doi.org/10.1063/1.4999011.
[9] M.A. Flores, E. Menéndez-Proupin, W. Orellana, J.L. Peña, Sn-doped CdTe as promising intermediate-band photovoltaic material, J. Phys. D Appl. Phys. 50 (2017), https://doi.org/10.1088/1361-6463/50/3/035501, 035501.
[10] W. Jantsch, G. Hendorfer, Characterization of deep levels in CdTe by photo-EPR and related techniques, J. Cryst. Growth 101 (1990) 404–413, https://doi.org/10.1016/0022-0248(90)91004-A.
[11] A. Luque, A. Martí, C. Stanley, Understanding intermediate-band solar cells, Nat. Photonics 6 (2012) 146–152, https://doi.org/10.1038/nphoton.2012.1.
[12] W. Shockley, W.T. Read, Statistics of the recombinations of holes and electrons, Phys. Rev. 87 (1952) 835–842, https://doi.org/10.1103/PhysRev.87.835.
[13] R.N. Hall, Electron-hole recombination in germanium, Phys. Rev. 87 (1952), https://doi.org/10.1103/PhysRev.87.387, 387–387.
[14] J.J. Krich, B.I. Halperin, A. Aspuru-Guzik, Nonradiative lifetimes in intermediate band materials - absence of lifetime recovery, J. Appl. Phys. 112 (2012), https://doi.org/10.1063/1.4732085, 013707.
[15] A. Luque, A. Martí, E. Antolín, C. Tablero, Intermediate bands versus levels in non-radiative recombination, Phys. B Condens. Matter 382 (2006) 320–327, https://doi.org/10.1016/j.physb.2006.03.006.
[16] D.J. Chadi, Predictor of p-type doping in II-VI semiconductors, Phys. Rev. B 59 (1999) 181–183, https://doi.org/10.1103/PhysRevB.59.15181.
[17] A.M. Ruiz, O. Vigil, E. Saucedo, G.B.V. Contreras-Puente, Bi doped CdTe: increasing potentialities of CdTe based solar cells, J. Phys. Condens. Matter 18 (2006) 7163–7169, https://doi.org/10.1088/0953-8984/18/31/011.
[18] R.E. Kremer, W.B. Leigh, Deep levels in CdTe, J. Cryst. Growth 86 (1998) 490–496, https://doi.org/10.1063/1.366946.
[19] B.E. McCandless, W.A. Buchanan, C.P. Thompson, G. Sriramagiri, R.J. Lovelett, J. Duenow, D. Albin, S. Jensen, E. Colegrove, J. Moseley, H. Moutinho, S. Harvey, overcoming carrier concentration limits in polycrystalline CdTe thin films with in situ doping, Sci. Rep. 8 (2018) 14519, https://doi.org/10.1038/s41598-018-32746-y.
[20] D.R. Lide, CRC Handbook of Chemistry and Physics, CRC Press, Boca Raton, 2005.

[21] R.M. Badger, A relation between internuclear distances and bond force constants, J. Chem. Phys. 2 (1934) 128–131, https://doi.org/10.1063/1.1749433.
[22] B.H. Torrie, Raman spectrum of Tellurium, Solid State Commun. 8 (1970) 1899–1901, https://doi.org/10.1016/0038-1098(70)90343-1.
[23] R.N. Zitter, Raman detection of tellurium layers on surfaces of CdTe, Surf. Sci. 28 (1971) 335–338, https://doi.org/10.1016/0039-6028(71)90103-8.
[24] M. Dharmadasa, O.K. Echendu, F. Fauzi, N.A. Abdul-Manaf, O.I. Olusola, H. I. Salim, M.L. Madugu, A.A. Ojo, Improvement of composition of CdTe thin films during heat treatment in the presence of CdCl2, J. Mater. Sci. Mater. Electron. 28 (2017) 2343–2352, https://doi.org/10.1007/s10854-016-5802-9.
[25] Ş. Ţălua, R.P. Yadavb, O. Šikc, D. Sobolac, How topographical surface parameters are correlated with CdTe monocrystal surface oxidation, Mater. Sci. Semicond. Process. 85 (2018) 15–23, https://doi.org/10.1016/j.mssp.2018.05.030.
[26] S. Acharya, J. Pandey, A. Soni, Soft phonon modes driven reduced thermal conductivity in self-compensated Sn1.03Te with Mn doping, Appl. Phys. Lett. 109 (2016), https://doi.org/10.1063/1.4963728, 133904.
[27] M.A. Tagliente, M. Penza, M. Gusso, A. Quirini, Characterisation of ZnS: Mn thin films by Rietveld refinement of Bragg–Brentano X-ray diffraction patterns, Thin Solid Films 353 (1999) 129–136, https://doi.org/10.1016/S0040-6090(99)00395-8.
[28] G. Gordillo, J.M. Flórez, L.C. Hernández, Preparation and characterization of CdTe thin films deposited by CSS, Sol. Energy Mater. Sol. Cells 37 (1995) 273–281, https://doi.org/10.1016/0927-0248(95)00020-8.
[29] T.L. Chu, Thin film cadmium telluride solar cells by two chemical vapor deposition techniques, Sol. Cells 23 (1988) 31–48, https://doi.org/10.1016/0379-6787(88)90005-1.
[30] E. Jaffe, Computational study of Ge and Sn doping of CdTe, J. Appl. Phys. 99 (2006), https://doi.org/10.1063/1.2168237, 033704.
[31] G. Quiñones-Galván, A. Guillén-Cervantes, E. Campos-González, J. Santos-Cruz, S. A. Mayén-Hernández, M. Olvera, O. Zelaya-Angel, G. Contreras-Puente, F. Moure-Flores, Structural properties of Sn-doped CdTe thin films grown by pulsed laser deposition using powder as target, J. Laser Appl. 28 (2016), https://doi.org/10.2351/1.4954202, 032012.
[32] M.A. Flores, W. Orellana, E. Menéndez-Proupin, First-principles DFT +GW study of the Te antisite in CdTe, Comput. Mater. Sci. 125 (2016) 176–182, https://doi.org/10.1016/j.commatsci.2016.08.044.
[33] R. Bhattacharya, B. Pal, B. Bansal, On conversion of luminescence into absorption and the van Roosbroeck-Shockley relation, Appl. Phys. Lett. 100 (2012), https://doi.org/10.1063/1.4721495, 222103.